# Fast imaging of DNA motion reveals distinct sub-diffusion regimes at the site of DNA damage

Judith Miné-Hattab[1,2,3,*,#], Vincent Recamier[1,6,*], Ignacio Izeddin[1,4], Rodney Rothstein[2], Xavier Darzacq[1,5#]

[1] Institut de Biologie de l'Ecole Normale Superieure (iBENS), Paris 75005, France

[2] Department of Genetics & Development, Columbia University Medical Center, New York, NY 10032, USA

[3] Nuclear Dynamics, CNRS UMR 3664, Institut Curie, Paris 75005, France

[4] Institut Langevin, ESPCI Paris Tech, CNRS UMR 7587, PSL Research University, 75005 Paris, France

[5] Division of Genetics, Genomics & Development, Department of Molecular and Cell Biology, University of California, Berkeley, Berkeley, CA 94720, USA

[6] Laboratory Imaging, s. r. o. Za Drahou 171/17 102 00 Praha 10, Czech Republic

Contact:

judith.mine@curie.fr

darzacq@berkeley.edu

[*] equal contribution

# corresponding authors

## ABSTRACT

The dynamic organization of genes inside the nucleus is an important determinant for their biological function. Using ultra-fast microscopy in living *S. cerevisiae* cells and improved analysis of DNA mean square displacements, we observe that DNA motion is sub-diffusive at time scales ranging from 10 ms to a few minutes. These distinct sub-diffusive regimes simultaneously drive DNA motion differently at each time scale. In response to a double-strand break, a damaged locus is more mobile at large time scales but, surprisingly, the broken DNA imaged at millisecond intervals is much less mobile. Such a change in the sub-diffusion mode dramatically modifies how DNA explores its surrounding nuclear space. We propose a model in which stiffening of the damaged DNA ends by the repair complex reduces its mobility locally, but allows significant nuclear exploration at longer time scales due to an enhanced ability to traverse the DNA meshwork.

## INTRODUCTION

The dynamic organization of the nuclear genome is essential for many biological processes and is often altered in cells from diseased tissue (Misteli, 2010). Recent advances in live cell imaging make it possible to visualize the dynamic organization of chromosomal loci inside living nuclei (Bronshtein Berger et al., 2013 ). One method to characterize DNA mobility consists of fluorescently marking chromosomal loci, measuring their displacement over time and calculating their mean square distance (MSD) (Meister et al., 2010). The MSD curve represents the amount of space a locus has explored in the nucleus and its shape reveals the nature of DNA motion. The mode of diffusion of a moving object drastically changes the way it explores the available space and the time to reach a specific target destination (Guerin et al., 2012). Thus, to understand the kinetics of co-localization between two biological entities, it is important to accurately determine how these entities diffuse. For example, when a chromosomal locus is confined inside a sub-volume of the nucleus, the motion is called *confined diffusion* and the MSD exhibits a plateau (Marshall et al., 1997). When the force or structure that restricts the motion is not a simple confinement but is modulated in time and space with scaling properties, the motion is *sub-diffusive* (Barkai et al., 2012, Metzler et al.,

2014). In this case, sub-diffusive loci are constrained by their environment but unlike confined loci, they can diffuse without boundary and thus reach further targets if given enough time. For sub-diffusive motion, the MSD exhibits a power law ($MSD \sim At^{\alpha}$), where $\alpha$, the anomalous exponent, is smaller than 1. The anomalous exponent $\alpha$ is linked to the degree of recurrence of DNA exploration, i.e., the number of times a DNA locus reiteratively scans neighboring regions before reaching a distant position (Ben-Avraham, 2000). The anomalous diffusion coefficient *A* represents the amplitude of DNA motion; it is proportional to the diffusion coefficient only in the case of normal diffusion (when $\alpha=1$), which is rarely observed in biological systems (Barkai et al., 2012). Previous DNA mobility studies reported confined diffusion (Marshall et al., 1997, Heun et al., 2001, Masui et al., 2011, Backlund et al., 2015) while others have reported anomalous diffusion (Weber et al., 2010, Hajjoul et al., 2013, Lucas et al., 2014, Backlund et al., 2015, Burnecki et al., 2012). Despite many studies, no consensus has yet been reached to describe the nature of DNA motion.

In the presence of double strand breaks (DSB) in *S. cerevisiae* and some mammalian cell lines, DNA mobility is dramatically increased (Haber and Leung, 1996, Neumann et al., 2012, Miné-Hattab and Rothstein, 2012, Dion et al., 2012, Jakob et al., 2011, Chiolo et al., 2011, Dimitrova et al., 2008, Roukos et al., 2013). In diploid yeast, increased mobility following DSBs likely favors pairing between homologs during repair by homologous recombination (HR) (Miné-Hattab and Rothstein, 2012). On the other hand, in haploid cells, increased mobility in response to DSBs is thought to promote ectopic repair events (Neumann et al., 2012). Similarly, in mouse cells, DSBs exhibiting increased mobility are the source of chromosomal translocations (Roukos et al., 2013). Thus, increased DNA mobility in response to DNA damage acts as a double-edged sword since it promotes homologous pairing but in some cases also it leads to potentially mutagenic DNA repair events.

As chromosome mobility is an important facet of the DNA damage response, investigating the nature of DNA diffusion in the context of repair is essential to understand how cells maintain their genome integrity. Here we have investigated DNA mobility at different time scales ranging from milliseconds to minutes using ultra-fast microscopy in living *S. cerevisiae* cells. We observe that DNA motion is sub-diffusive at time scales ranging from milliseconds to a few minutes, with an anomalous exponent of 0.5 in most of the conditions. However, in some cases, different anomalous regimes are observed depending on

the time scale, the cell ploidy or the presence of a DSB. For example, the anomalous diffusion coefficient A of the MSD varies significantly between haploids and diploids. In addition, damaged DNA loci in diploid cells exhibit increased mobility together with an anomalous exponent larger than 0.5 at the seconds and minute time scales. Interestingly, at shorter time scales (less than 1s), we observe reduced mobility of the damaged ends. We propose a model in which the stiffening of damaged, Rad51-bound DNA leads to a reduction in mobility at short time scales, but allows significant exploration at longer time scales due to an enhanced ability to traverse the DNA meshwork. In a sense, damaged DNA ends behave like a needle to help it search through a ball of yarn: the stiffening of the damaged ends makes it uniquely able to penetrate and explore the entangled chromatin network efficiently.

## RESULTS

### DNA mobility in haploid and diploid cells exhibits different anomalous regimes

To characterize DNA dynamics at different time scales, we first used haploid cells with a locus fluorescently marked by the insertion of a tet-Operator (*tetO*) array at *URA3* (chromosome V). This *tetO* array is bound by Tet-Repressors, which are fused to red fluorescent proteins (TetR-RFP). We also tagged a structural component of the spindle pole body (SPB) with yellow fluorescent protein, Spc110-YFP, to serve as a marker of the relative nuclear position and to correct for drifting during image acquisition for time intervals longer than 100 ms. Rad52, an essential homologous recombination protein, is fused to cyan fluorescent protein (CFP) to detect the presence of DSB (Fig. 1A and 1B) (Miné-Hattab and Rothstein, 2012). We selected early S-phase cells with a single SPB (approximately 10% of the total population), and where the *tetO*/TetR-RFP and Spc110-YFP foci are in the same focal plane. We recorded 2-dimensional movies of these cells (see supplementary movie 1). To avoid cells with spontaneous DNA damage, we ensured that they did not contain a Rad52 focus. Cells were imaged at three time scales:

i) 10 ms time intervals (5 ms exposure time in RFP, no YFP data were acquired since the global movement of the nucleus is negligible during this interval),

ii) 100 ms time intervals (50 ms exposure in RFP followed by the same exposure in YFP to track the *URA3* locus and the SPB respectively),

iii) 1000 ms time intervals (500 ms exposure in RFP followed by the same exposure time in YFP).

From the drift-corrected *x* and *y* coordinates of the *tetO*/TetR-RFP, we calculated the ensemble-averaged MSD using up to 1/3 of the longest trajectory (from 70 to 100 time points). At the three time scales examined, the MSD curves show bending in linear scale suggesting sub-diffusion (Fig. 1C, 1D and 1E). The MSDs at the three time scales are plotted together in log-log scale to allow their simultaneous visualization (Fig. 1F). Since a power law curve can be mistaken for an exponential form that would account for confined diffusion, we used several methods to confirm the sub-diffusive nature of DNA motion (Fig. S1). Experimental MSDs are altered by several artifacts (Backlund et al., 2015, Kepten et al., 2013); thus, we use an improved formula to fit MSD curves that takes into account locus mobility during image acquisition and limited position accuracy, the later (~ 90 nm) displays little variation between conditions (see Material and Methods, Supplementary Text 1 and 2 and Fig. S2). Our approach is similar to the one described in Kepten *et al.*, but also includes exposure time as an additional parameter. For 100 and 1000 ms exposure times, we obtain $MSD(t) \sim 0.012\ t^{0.5}$ (R2 = 0.996 for both conditions, Fig. 1D and E), similar to recent results by Hajjoul *et al.* ((Hajjoul et al., 2013), $MSD(t) \sim 0.011\ t^{0.5}$). However, we observe a different regime at 10 ms time intervals and find $MSD(t) \sim 0.011\ t^{0.38}$ (R2=0.999, Fig. 1C) suggesting that the regime defined by an anomalous exponent of 0.5 is not universal. Although we observe significant cell-to-cell variability (Fig. S3A, B and C), statistical analyses show that this discrepancy of the anomalous exponent is not due to an insufficient dataset (Fig. S3D, E, and F), and is also consistent with previous studies (Therizols et al., 2011, Bronstein et al., 2009).

We next applied the same experimental scheme to diploid cells containing a *tetO*/TetR-RFP array at one of the *URA3* loci and the Spc110-YFP marked SPB (Fig. 2A and B). Similar to our observations with haploid cells, diploids follow sub-diffusive motion, however, unlike haploids, a 0.5 anomalous exponent is observed at all-time scales (Fig. 2C, 2D and 2E). Strikingly, a significant decrease of the global MSD in diploids is seen compared to haploids at every exposure time investigated, due to lower values of the anomalous diffusion coefficient *A* (Fig. 2F). For diploids, we obtain $MSD(t) \sim 0.0075\ t^{0.5}$ at 10 and 100 ms time intervals (R2= 0.978 and 0.982). At large time scales (1000 ms time intervals), we

observe a different anomalous regime indicating a reduced mobility (MSD (t) ~ 0.0064 $t^{0.49}$, R2 = 0.982). Table 1 presents a summary of the results obtained in both haploids and diploids. Overall, the motion of the *URA3* locus is sub-diffusive for time scales ranging from milliseconds to minutes, and is well fit by a 0.5 anomalous exponent in most conditions. However, a universal regime is not sufficient to describe DNA motion. First, at the very short time scale (10 ms), the anomalous exponent drops to 0.38 in haploids; second, at all-time scales examined, diploid cells exhibit a lower MSD curve than haploids.

**Damaged DNA is less mobile at short time scales**

Previous studies have shown that the mobility of a damaged DNA locus increases when the motion is observed at 10 s time intervals in diploids (Miné-Hattab and Rothstein, 2012) and 1.5 s intervals in haploids (Dion et al., 2012). However, mobility after DNA damage at shorter time scales has never been investigated. Here, we measure, with unprecedented precision, the mobility of a single I-*Sce*I induced DSB in the same strains used in our previous study (Miné-Hattab and Rothstein, 2012) (Fig. 3). We used diploid cells containing the homologous *URA3* loci fluorescently marked with a *lacO*/LacI-YFP and a *tetO*/TetR-RFP array, respectively (Fig. 3A). To induce a single DSB, the strain contains an I-*Sce*I target site 4 kb from the *tetO*/TetR-RFP locus, as well as RAD52-CFP used as a marker for the presence of the DSB. Cells were incubated in 2% galactose for 90 minutes to induce the DSB and induction was stopped by adding 2% glucose. Note that the precise time of the Rad52 focus formation cannot be known; however, we always observed cells after the same incubation time (90 min), when Rad52 foci start to appear (Miné-Hattab and Rothstein, 2012). We selected S-phase cells harboring a single SPB and a Rad52 focus colocalizing with the *URA3* locus (*tetO*/TetR-RFP) in the SPB focal plane. We verified that the two homologous *URA3* loci were unpaired by choosing cells with a distant *URA3* homologue (*lacO*/LacI-YFP) (Fig. 3A and 3B). The *tetO* and SPB positions were measured over time in 2D and we calculated ensemble-averaged MSDs on these cells (Fig. 3C, D and E). Similar to our observations in the absence of DSBs, the damaged locus follows sub-diffusive motion. At the longest time scale (1000 ms), we find the highest values of $A$ and $\alpha$ in this study (MSD(t) ~ 0.0087 $t^{0.58}$, R2 = 0.994) consistent with the increased mobility previously reported at 10 s time intervals (Miné-Hattab and Rothstein, 2012, Dion et al., 2012). Surprisingly, the motion of the

damaged locus observed at shorter time intervals exhibits a lower amplitude and anomalous exponent than that seen in undamaged cells, signifying reduced mobility (MSD(t) ~ 0.0065 $t^{0.50}$, R2 = 0.974 and R2 = 0.992 at 100 and 10 ms time intervals respectively, Fig. 2E, 3C, D and Table 1). As a consequence, the MSD curve of the damaged locus crosses that of the undamaged one at time t~10s (Fig. 3F).

## DISCUSSION

### Multi time-scale microscopy reveals the composite nature of DNA motion

Previous studies have shown that DNA motion observed at large time scales (1.5 to 10 s time intervals) is confined within a sub-nuclear volume (Heun et al., 2001, Marshall et al., 1997, Miné-Hattab and Rothstein, 2012). In response to DSBs, DNA becomes more mobile and explores a larger nuclear volume (Miné-Hattab and Rothstein, 2012, Dion et al., 2012). Here, by investigating DNA motion at time scales 10, 100 and 1000 times faster, we find that the MSD curves do not exhibit a plateau indicating that the effect of confinement is not observed at these scales; instead, the MSD curves are in excellent agreement with a power law, MSD(t) ~ $At^{\alpha}$, a signature of anomalous diffusive motion (Barkai et al., 2012). The anomalous exponent α is linked to the degree of recurrence of the motion, low α corresponding to a locus that rescans neighboring loci many times in a highly recurrent manner (Ben-Avraham, 2000). The anomalous diffusion coefficient *A* reflects the amount of volume explored by a locus as a function of time (i.e., the amplitude of the motion). Interestingly, our data show a fundamental difference in DNA mobility between haploids and diploids. The anomalous diffusion coefficient *A* is nearly two times higher in haploids indicating that the *URA3* locus is more mobile in haploids. One possible explanation for this difference is that the chromatin in haploid cells is less dense.

In response to DNA damage, we find distinct anomalous regimes depending on the time scales, with both *A* and $\alpha$ increasing between the 100 ms and 1000 ms time intervals experiments (Fig. 3 and Table 1). At 1000 ms time intervals, the higher *A* together with the higher $\alpha$ of the damaged locus indicates that, following a DSB, the damaged locus moves with a larger amplitude and in a less redundant fashion (Table 1, A = 0.0087, α = 0.58 after DSB compared to 0.0064 and 0.49 before damage). On the other hand, the low anomalous

diffusion coefficient A of the damaged locus at 10 and 100 ms time intervals reflects reduced amplitude of the damaged DNA motion (Table 1, $A$ = 0.0065 after DSB compared to 0.0075 before). Overall, we show that, in the absence of DNA damage, a single mode of diffusion is not sufficient to describe DNA motion at different time scales. Instead, that motion is composed of several diffusion regimes that drive DNA simultaneously. Interestingly, in response to DSBs, the change in regimes at large time scales leads to increased exploration of the nuclear volume, while short time scales reveal reduced mobility locally.

**Origin of sub-diffusive motion**

Sub-diffusive motion has been observed in bacteria, yeast and human cells, with anomalous exponents ranging from 0.32 to 0.77 (Weber et al., 2010, Hajjoul et al., 2013, Lucas et al., 2014, Bronstein et al., 2009, Backlund et al., 2014). Even though different time scales were examined in these studies, none clearly showed the existence of multiple anomalous regimes with the exception of (Bronstein et al., 2009). In their study, they found that in U2OS cells, diffusion of telomeres is composed of two transient anomalous regimes at time scales ranging from 10 ms to 1.7 min ($\alpha = 0.32 \pm 0.12$ and $\alpha = 0.51 \pm 0.20$), and becomes close to Brownian at time scales greater than 5' (Bronstein et al., 2009). Their work emphasizes the importance of the time scale of observation for interpreting DNA motion. To understand the origin of anomalous sub-diffusion of DNA in the nucleus, several models have been proposed:

1) The nucleoplasm is modeled as a visco-elastic medium. Mathematical models of visco-elasticty are fractional Brownian motion (FBM) and fractional Langevin motion (FLM) (Metzler and Klafter, 2000). In these models, DNA is subjected to frictional forces that are not proportional to DNA velocity.
2) The nucleoplasm is modeled as a fractal. DNA loci are free explorers moving in a restricted geometry with scale-less properties imposed by nuclear crowding (Condamin et al., 2007).
3) The nucleoplasm is modeled as a polymer melt. DNA loci are represented by monomers whose motion is driven by the properties of this melt. Several polymer models have been suggested to describe DNA mobility, from diluted regimes (Rouse,

Zimm models (Andrews, 2014, Vasquez and Bloom, 2014) to a larger scale semi-diluted regime ("tube" model also called "blob" model (De Gennes, 1982)).

We did not consider the first two types of models because they do not predict different/distinct regimes. Since DNA is a polymer, we compared our experimental anomalous exponents to those obtained in the three polymer models referred to above. The "tube" model of De Gennes is the only one that predicts different regimes of anomalous diffusion arising in a polymer melt (De Gennes, 1982). This model predicts 3 anomalous diffusion regimes: the Rouse regime at a diluted scale (where $\alpha = 0.5$), the "relaxation of the coil" regime ($\alpha = 0.25$) followed by the "reptation" regime ($\alpha = 0.5$) at a semi-diluted scale and concentration where adjacent chains constrain the motion. Finally, it predicts Brownian diffusion ($\alpha = 1$) at the macroscopic scale. The reptation regime is obtained by averaging different conformations of polymer entanglements, thus it is the only model that takes into account potential cell-to-cell variability (De Gennes, 1982). This regime has been directly observed *in vitro* for constrained DNA melts (Perkins et al., 1994); moreover, in live U2OS cell experiments, diffusion of telomeres observed at 1 second time intervals may be explained by the reptation regime (Bronstein et al., 2009). Here, in most conditions, we find a 0.5 anomalous exponent. To explain this behavior, we favor the "reptation regime" *versus* the Rouse regime for the following 4 reasons: i) we observe an anomalous diffusion coefficient *A* in haploids that is double that of diploids: in the reptation regime, this difference in *A* would be well justified by a lower level of chromatin entanglements in haploids compared to diploids, whereas the Rouse regime does not explain it, ii) at the shortest time interval, haploids exhibit a regime with an anomalous exponent lower than 0.5, which may be a transition from *the relaxation of the coil* regime to the reptation regime, iii) we observe high cell-to-cell variability, as predicted by the reptation regime, and finally iv), modeling the stiffening of a polymer in the reptation regime leads to reduced mobility at smaller scales and increased mobility at larger scales (Faller and Müller-Plathe, 2008), ,which is consistent with our experimental observations on broken DNA after a DSB.

**Evidence of a local increased chromatin persistence length near the damaged site**

The changes in $A$ that we measured reveal valuable information on chromatin plasticity around the damaged locus. For example, in the Rouse and the reptation regimes, where $\alpha$ = 0.5, the anomalous diffusion coefficient $A$ negatively correlates with the chromatin persistence length, $L_p$ (Hajjoul et al., 2013). Indeed, using the equation $A \sim 1/\sqrt{L_p}$ from the Rouse model, Hajjoul *et al.* extracted a chromatin persistence length of ~5 nm from their MSD measurements (Hajjoul et al., 2013). On the other hand, for the reptation regime, to our knowledge, there is no consensus on the exact equation linking $A$ and the persistence length $L_p$. However, simulations of this regime reveal an anti-correlation between $A$ and $L_p$ (Faller and Müller-Plathe, 2008), similar to that seen for the Rouse regime. Since there is no explicit formula linking $A$ and $L_p$ for the reptation regime, we can only discuss qualitatively the relative changes of persistence lengths observed. Thus, at 10 or 100 ms time intervals, where the anomalous exponent $\alpha$ is 0.5, we find that the anomalous diffusion coefficient $A$ decreases from 0.0075 to 0.0065 in response to a DSB (Fig. 3 and Table 1). This change in $A$ is consistent with a local increase in persistence length due to stiffening of the damaged DNA ends by the repair proteins, as previously observed *in vitro* for the Rad51 nucleo-filament (Mine et al., 2007, Lee et al., 2013).

**The "needle in a ball of yarn" model**

Using our observations, we formulate a model in which the damaged DNA, stiffened by the repair complex, exhibits reduced mobility at small time scales, but simultaneously exhibits increased mobility at longer ones. By stiffening the damaged DNA end, the repair machinery acts like a needle to help it search through the chromatin mesh, likened to a "ball of yarn" (Figure 4). The repair complex reduces the local mobility of the damaged locus and therefore the relaxing time of the broken chain. At short time scales, the stiffening of the Rad51-bound DNA leads to a reduction of mobility. However, concomitantly, the Rad51-DNA nucleo-filament enhances its ability to pass through the DNA meshwork and escape adjacent obstacles more efficiently as observed at larger scales. This model explains the different regimes of diffusion that co-exist at different time scales and point out the central role of Rad51 in tuning the motion of the damaged DNA ends. More generally, we propose that DNA diffusion is controlled by the local conformation of chromatin, e.g., the level of

entanglement as described in the "tube model" (De Gennes, 1982). Our observations suggest that local chromatin conformations are different between haploids and diploids and at the vicinity of a DSB. It would be very informative for example to visualize DNA organization at the nanoscale level *in vivo* in these different situations to observe whether local DNA conformations are affected. It will also be interesting to examine other biological processes at different time scales to see whether the multi-scale exploration of space that we observe here is a general property that allows a more efficient sampling of the environment.

## MATERIALS AND METHODS:

### Strains

All strains used in this work are isogenic to *RAD5+* W303 (Zhao et al., 1998) derivatives (Supplementary Table S2).

### Cell culture and DSB induction

Before microscopy, cells were grown to early log phase in 4 ml cultures of SC medium + 100 mg $l^{-1}$ adenine + 2% raffinose at 23°C overnight. In the morning, 2% galactose was added to the culture for 90 minutes to induce a single DSB at the I-*Sce*I cut-site. Cells were then pelleted, washed in SC + 100 mg $l^{-1}$ adenine medium + 2% glucose to stop DSB induction and placed on a 1.4% agarose slab for microscopy (Miné-Hattab and Rothstein, 2012). During the DSB induction, the I-*Sce*I cutting starts to occur after 30 minutes of induction but the first Rad52 foci colocalizing with the *tetO* array are visible by microscopy after 90 minutes of induction and can last more than 30 minutes (Miné-Hattab and Rothstein, 2012). Thus, the time of the DSB formation cannot be known precisely. To measure DNA mobility of the damaged locus, we select cells harboring a Rad52 focus after 90 minutes of induction. The DSB is not necessarily formed at the same time in all cells examined: however, since we measure time-ensemble averaged MSDs on several cells, the presence of distinct anomalous regimes does not reflect different mobilities dependent on time after DSB induction, but is solely due to the different time scales used to observe the locus.

**Microscopy**

Imaging of single DNA loci was performed on an inverted microscope Nikon Ti Eclipse (Nikon Instruments, Tokyo, Japan), with a high numerical aperture objective (1.49 NA) and 100X magnification. We used a perfect focus system (Nikon) designed to avoid drift on the Z-axis of the optical system and keep the cells in focus. The excitation laser beams (514 nm and 561 nm) were coupled into an optical fiber and focused in the back focal plane of the objective using an appropriate dual band dichroic (Semrock Di01-R488/561-25x36). Experiments were acquired with alternating pulsed excitation for the 514 nm laser and the 561 nm laser, respectively. Fluorescence emission from either YFP or RFP fluorescent proteins was filtered with a dual band emission filter with windows centered at 523 nm (45 nm bandpass) and 610 nm (45 nm bandpass) (Semrock FF01-523/610-25). The pixel size of the EMCCD is 16 μm (iXon 897 Andor Technology, Belfast, Ireland), producing a pixel size of 160 nm after magnification. For the experiments at 5 ms acquisition time, we imaged a small region of interest containing the cell of interest, which allowed us to obtain acquisition rates as fast as 200 Hz (5 ms per frame).

**Image analysis**

We detected and tracked the *x* and *y* positions of the DNA loci using a home-made program inspired by the MTT tracking software (Serge et al., 2008). From the *x* and *y* positions of the DNA locus over time, we computed the time-ensemble averaged Mean Square Displacement (MSD) using the formula:

$MSD(\tau) = \langle \Delta \mathbf{r}(\tau)^2 \rangle = \langle [\mathbf{r}(t+\tau) - \mathbf{r}(t)]^2 \rangle$, where $\mathbf{r}(t)$ is the 2D-position of the particle at time $t$, and $\tau$ is the lag time between two positions of the particle used to calculate the displacement $\Delta \mathbf{r}(\tau) = \mathbf{r}(t+\tau) - \mathbf{r}(t)$. The symbol $< >$ represents a time-average over $t$ and over locus trajectories acquired from different cells. The error bar is the 95% confidence interval.

We confirmed the anomalous nature of the motion using several methods (Fig. S1). The theoretical MSD of a sub-diffusive motion is a power law, $MSD(t) = At^{\alpha}$. However, experimental MSDs are altered from their theoretical shape due to various experimental limitations such as limited position accuracy or locus mobility during each image acquisition (Kepten et al., 2013, Backlund et al., 2015). Those limitations add an offset term, *b*, to the

experimental asymptotic MSD, compared to the theoretical one: $MSD_{experimental}(t) = At^{\alpha} + b$ (Hughes, 1995) (see Supplementary Text 1). Here, we derived a versatile formula of the MSD to compute this offset *b*, allowing us to accurately fit our experimental MSD derived from different acquisition schemes (see equation 1 from Supplementary Text 1, and Fig. S2). Our approach is more general than the one described in Kepten *et al*. (2013) since it also includes the exposure time as an additional parameter.

## AUTHOR CONTRIBUTIONS:

JM-H : designed and performed the experiments, analyzed and interpreted the data, wrote the manuscript, coordinated the project.

VR : analyzed and interpreted the data, co-wrote the manuscript.

II : helped in the conception of the experiments, helped in the interpretation the data and revised the manuscript.

RR : interpreted the data, co-wrote the paper.

XD : helped in the conception of the experiments, helped in the interpretation of the data and coordinated the project.

## ACKOWLEDGMENTS:

We would like to thank Leonid Mirny, Angela Taddei, Maxime Dahan and Yaron Shav-Tal for fruitful discussions about this work. We would like to thank also Christophe Zimmer, Eldad Kepten, Peter Thorpe and Chloé Guedj for fruitful comments on this manuscript. This work was funded by a Marie Curie International Outgoing Fellowship (JM-H), the ANR-12-PDOC-0035-01 (JM-H), the Fondation pour la Recherche Médicale (Foundation for Medical Research in France) (VR), National Institutes of Health (GM50237 and GM67055) (RR).

## REFERENCES:

ANDREWS, S. S. 2014. Methods for modeling cytoskeletal and DNA filaments. *Phys Biol,* 11**,** 011001.

BACKLUND, M. P., JOYNER, R. & MOERNER, W. E. 2015. Chromosomal locus tracking with proper accounting of static and dynamic errors. *Phys Rev E Stat Nonlin Soft Matter Phys,* 91**,** 062716.

BACKLUND, M. P., JOYNER, R., WEIS, K. & MOERNER, W. E. 2014. Correlations of three-dimensional motion of chromosomal loci in yeast revealed by the double-helix point spread function microscope. *Mol Biol Cell,* 25**,** 3619-29.

BARKAI, E., GARINI, Y. & METZLER, R. 2012. Strange kinetics of single molecules in living cells. *Physics today,* 65**,** 29-35.

BEN-AVRAHAM, D. H., S. 2000. Diffusion and reactions in fractals and disordered systems *Cambridge University Press*.

BRONSHTEIN BERGER, I., KEPTEN, E. & GARINI, Y. 2013 Single-Particle Tracking for Studying the Dynamic Properties of Genomic Regions in Live Cells. *Methods Mol Biol,* 1042**,** 139-51.

BRONSTEIN, I., ISRAEL, Y., KEPTEN, E., MAI, S., SHAV-TAL, Y., BARKAI, E. & GARINI, Y. 2009. Transient anomalous diffusion of telomeres in the nucleus of mammalian cells. *Physical review letters,* 103**,** 018102.

BURNECKI, K., KEPTEN, E., JANCZURA, J., BRONSHTEIN, I., GARINI, Y. & WERON, A. 2012. Universal algorithm for identification of fractional Brownian motion. A case of telomere subdiffusion. *Biophys J,* 103**,** 1839-47.

CHIOLO, I., MINODA, A., COLMENARES, S. U., POLYZOS, A., COSTES, S. V. & KARPEN, G. H. 2011. Double-strand breaks in heterochromatin move outside of a dynamic HP1a domain to complete recombinational repair. *Cell,* 144**,** 732-44.

CONDAMIN, S., BENICHOU, O. & KLAFTER, J. 2007. First-passage time distributions for subdiffusion in confined geometry. *Phys Rev Lett,* 98**,** 250602.

DE GENNES, P. G. 1982. Kinetics of diffusioncontrolled processes in dense polymer systems. II.Effects of entanglements. *The Journal of Chemical Physics,* 76**,** 3322-26.

DIMITROVA, N., CHEN, Y. C., SPECTOR, D. L. & DE LANGE, T. 2008. 53BP1 promotes non-homologous end joining of telomeres by increasing chromatin mobility. *Nature,* 456**,** 524-8.

DION, V., KALCK, V., HORIGOME, C., TOWBIN, B. D. & GASSER, S. M. 2012. Increased mobility of double-strand breaks requires Mec1, Rad9 and the homologous recombination machinery. *Nat Cell Biol,* 14**,** 502-9.

FALLER, R. & MÜLLER-PLATHE, F. 2008. Chain stiffness intensifies the reptation characteristics of polymer dynamics in the melt. *Chemphyschem,* 2**,** 180-4.

GUERIN, T., BENICHOU, O. & VOITURIEZ, R. 2012. Non-Markovian polymer reaction kinetics. *Nat Chem,* 4**,** 568-73.

HABER, J. E. & LEUNG, W. Y. 1996. Lack of chromosome territoriality in yeast: promiscuous rejoining of broken chromosome ends. *Proc Natl Acad Sci U S A,* 93**,** 13949-54.

HAJJOUL, H., MATHON, J., RANCHON, H., GOIFFON, I., MOZZICONACCI, J., ALBERT, B., CARRIVAIN, P., VICTOR, J. M., GADAL, O., BYSTRICKY, K. & BANCAUD, A. 2013. High-throughput chromatin motion tracking in living yeast reveals the flexibility of the fiber throughout the genome. *Genome Res,* 23**,** 1829-38.

HEUN, P., LAROCHE, T., SHIMADA, K., FURRER, P. & GASSER, S. M. 2001. Chromosome dynamics in the yeast interphase nucleus. *Science,* 294**,** 2181-6.

HUGHES, B. D. 1995. Random Walks and Random Environments: Volume 1: Random Walks. *Oxford science publications*.

JAKOB, B., SPLINTER, J., CONRAD, S., VOSS, K. O., ZINK, D., DURANTE, M., LOBRICH, M. & TAUCHER-SCHOLZ, G. 2011. DNA double-strand breaks in heterochromatin elicit fast repair protein recruitment, histone H2AX phosphorylation and relocation to euchromatin. *Nucleic Acids Res,* 39**,** 6489-99.

KAYE, J. A., MELO, J. A., CHEUNG, S. K., VAZE, M. B., HABER, J. E. & TOCZYSKI, D. P. 2004. DNA breaks promote genomic instability by impeding proper chromosome segregation. *Curr Biol,* 14**,** 2096-106.

KEPTEN, E., BRONSHTEIN, I. & GARINI, Y. 2013. Improved estimation of anomalous diffusion exponents in single-particle tracking experiments. *Phys Rev E Stat Nonlin Soft Matter Phys,* 87**,** 052713.

LEE, M., LIPFERT, J., SANCHEZ, H., WYMAN, C. & DEKKER, N. H. 2013. Structural and torsional properties of the RAD51-dsDNA nucleoprotein filament. *Nucleic Acids Res,* 41**,** 7023-30.

LISBY, M., ANTUNEZ DE MAYOLO, A., MORTENSEN, U. H. & ROTHSTEIN, R. 2003. Cell cycle-regulated centers of DNA double-strand break repair. *Cell Cycle,* 2**,** 479-83.

LOBACHEV, K., VITRIOL, E., STEMPLE, J., RESNICK, M. A. & BLOOM, K. 2004. Chromosome fragmentation after induction of a double-strand break is an active process prevented by the RMX repair complex. *Curr Biol,* 14**,** 2107-12.

LUCAS, J. S., ZHANG, Y., DUDKO, O. K. & MURRE, C. 2014. 3D trajectories adopted by coding and regulatory DNA elements: first-passage times for genomic interactions. *Cell,* 158**,** 339-52.

MARSHALL, W. F., STRAIGHT, A., MARKO, J. F., SWEDLOW, J., DERNBURG, A., BELMONT, A., MURRAY, A. W., AGARD, D. A. & SEDAT, J. W. 1997. Interphase chromosomes undergo constrained diffusional motion in living cells. *Curr Biol,* 7**,** 930-9.

MASUI, O., BONNET, I., LE BACCON, P., BRITO, I., POLLEX, T., MURPHY, N., HUPE, P., BARILLOT, E., BELMONT, A. S. & HEARD, E. 2011. Live-cell chromosome dynamics and outcome of X chromosome pairing events during ES cell differentiation. *Cell,* 145**,** 447-58.

MEISTER, P., GEHLEN, L. R., VARELA, E., KALCK, V. & GASSER, S. M. 2010. Visualizing yeast chromosomes and nuclear architecture. *Methods Enzymol,* 470**,** 535-67.

METZLER, R., JEON, J. H., CHERSTVY, A. G. & BARKAI, E. 2014. Anomalous diffusion models and their properties: non-stationarity, non-ergodicity, and ageing at the centenary of single particle tracking. *Phys Chem Chem Phys,* 16**,** 24128-64.

METZLER, R. & KLAFTER, J. 2000. The random walk's guide to anomalous diffusion: a fractional dynamics approach. *Physics Reports,* 339**,** 1-77.

MINE, J., DISSEAU, L., TAKAHASHI, M., CAPPELLO, G., DUTREIX, M. & VIOVY, J. L. 2007. Real-time measurements of the nucleation, growth and dissociation of single Rad51-DNA nucleoprotein filaments. *Nucleic Acids Res,* 35**,** 7171-87.

MINÉ-HATTAB, J. & ROTHSTEIN, R. 2012. Increased chromosome mobility facilitates homology search during recombination. *Nat Cell Biol,* 14**,** 510-7.

MISTELI, T. 2010. Higher-order genome organization in human disease. *Cold Spring Harb Perspect Biol,* 2**,** a000794.

NEUMANN, F. R., DION, V., GEHLEN, L. R., TSAI-PFLUGFELDER, M., SCHMID, R., TADDEI, A. & GASSER, S. M. 2012. Targeted INO80 enhances subnuclear chromatin movement and ectopic homologous recombination. *Genes Dev,* 26**,** 369-83.

PERKINS, T. T., SMITH, D. E. & CHU, S. 1994. Direct observation of tube-like motion of a single polymer chain. *Science,* 264**,** 819-22.

ROUKOS, V., VOSS, T. C., SCHMIDT, C. K., LEE, S., WANGSA, D. & MISTELI, T. 2013. Spatial dynamics of chromosome translocations in living cells. *Science,* 341**,** 660-4.

SERGE, A., BERTAUX, N., RIGNEAULT, H. & MARGUET, D. 2008. Dynamic multiple-target tracing to probe spatiotemporal cartography of cell membranes. *Nat Methods,* 5**,** 687-94.

THERIZOLS, P., DUONG, T., DUJON, B., ZIMMER, C. & FABRE, E. 2011. Chromosome arm length and nuclear constraints determine the dynamic relationship of yeast subtelomeres. *PNAS,* 107**,** 2025–2030.

VASQUEZ, P. A. & BLOOM, K. 2014. Polymer models of interphase chromosomes. *Nucleus,* 5**,** 376-90.

WEBER, S. C., SPAKOWITZ, A. J. & THERIOT, J. A. 2010. Bacterial chromosomal loci move subdiffusively through a viscoelastic cytoplasm. *Phys Rev Lett,* 104**,** 238102.

ZHAO, X., MULLER, E. G. & ROTHSTEIN, R. 1998. A suppressor of two essential checkpoint genes identifies a novel protein that negatively affects dNTP pools. *Mol Cell,* 2**,** 329-40.

## FIGURES LEGEND

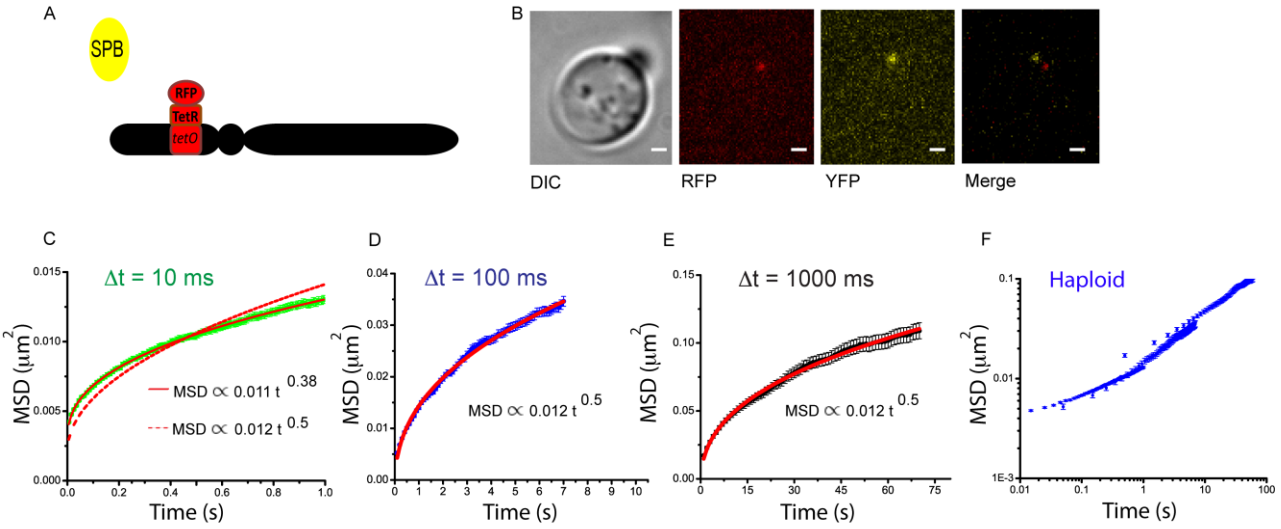


**Figure 1. Mobility in haploid cells**

(**A**) Schematic of the haploid strain. Haploid cells (W9562-1A) contain a *tet*O array (3x 112 copies) at the *URA3* locus (chromosome V). In addition, TetR and Spc110 proteins are tagged with RFP and YFP, respectively. S-phase cells with the *tet*O array and the SPB in the same focal plan are selected and the *tet*O spot is tracked in 2D over time using the SPB as a reference. (**B**) Typical DIC, RFP, YFP and merge images of the cells. The scale bar represents 1 μm. (**C**) Time and ensemble MSD of the *tet*O locus with a 5 ms exposure time at 10 ms time intervals in haploid cells. All MSDs were calculated from 13 to 70 trajectories, depending on the conditions. The error bars show the standard deviation of the mean of the squared displacement. The curve was fit to a function $f(t)=At^{\alpha}+b$ using least square sum as the criterion, according to equation 1 from Supplementary Text 1 and the protocol described in Supplementary Text 2. The standard deviations on parameters $A$ and $\alpha$ are given the Table 1. (**D**) Time and ensemble MSD of the *tet*O locus with a 50 ms exposure time at 100 ms time intervals in haploid cells. The dotted line displays the fit of the MSD curve using a constrained fit with $A$ = 0.012 and $\alpha$ = 0.5, similar to that found at 100 and 1000 ms time intervals. As shown by the poor quality of the fit, DNA failed to follow this regime. Plain lines display an unconstrained fit. (**E**) Time and ensemble MSD of the *tet*O locus with a 500 ms exposure time at 1000 ms time intervals in haploid cells. (**F**) Merge of the 3 time scales (Fig. 1C, 1D and 1E) plotted in log-log scale (black: diploids and blue: haplo

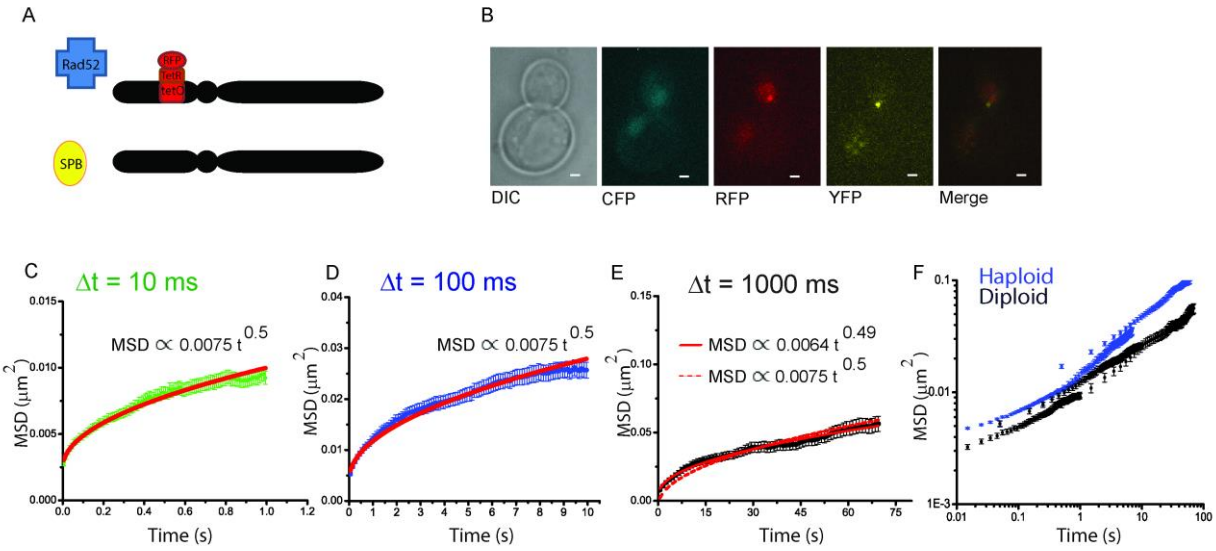


**Figure 2. Mobility in diploid cells at different time scales**

(**A**) Schematic of the strain: W9562 cells are diploids containing a *tet*O array (3x 112 copies) inserted at *URA3* (chromosome V). In addition, the Rad52, TetR and Spc110 proteins are tagged with CFP, RFP and YFP, respectively. Cells with the *tet*O locus and the SPB in the same focal plane are selected and the *tet*O locus is tracked in 2D over time using the SPB as a reference. (**B**) Typical transmitted, CFP, RFP, YFP and merge images of the cells used for the experiment. A single z-section is shown. The experiment is performed on S-phase cells in the absence of a DSB as shown by the absence of a Rad52 focus. The scale bar is 1 μm. (**C**) Time and ensemble MSD of the *tet*O locus measured with a 5 ms exposure time at 10 ms time intervals. MSDs were calculated as described in Fig. 1. (**D**) Time and ensemble MSD of the *tet*O locus measured with a 50 ms exposure time at 100 ms time intervals. (**E**) Time and ensemble MSD of the *tet*O locus measured with a 500 ms exposure time at 1000 ms time intervals. (**F**) Merge of the 3 time scales (Fig.2C, 2D and 2E) plotted in log-log scale.

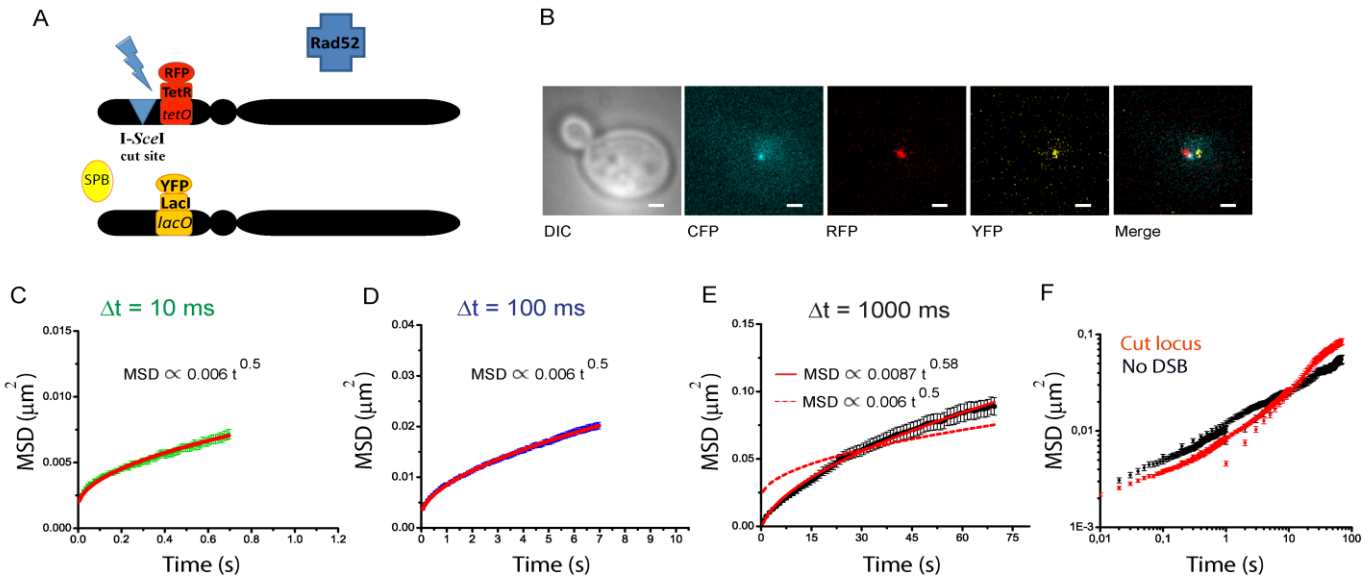


**Figure 3. Mobility in diploid cells in the presence of a single I-*Sce*I induced DSB at different time scales**

(**A**) Schematic of the strain used for the induction of a single DSB in diploid cells. Diploid cells (W9641) contain both a *tet*O array (3x 112 copies) at *URA3* (chromosome V) and a *lac*O array (256 copies) at *URA3* on the other homologue. The Rad52, TetR and LacI proteins are fused with CFP, RFP and YFP, respectively. A single I-*Sce*I cut-site is located 4 kbases from the *tetO* array. A galactose-inducible I-*Sce*I inserted at the *LYS2* locus allows regulated induction of a single DSB under galactose control (Miné-Hattab and Rothstein, 2012). (**B**) Typical transmitted, CFP, RFP, YFP and merge images of the cells after 90 minutes of galactose induction. A single z-section is shown. Only S-phase cells containing a Rad52 focus co-localizing with the *tet*O locus and a distant *lac*O focus are selected. The scale bar is 1 μm. (**C**) Time and ensemble MSD of the *tet*O locus measured with a 5 ms exposure time at 10 ms time intervals after induction of a single DSB. (**D**) MSD of the *tet*O locus measured with a 50 ms exposure time at 100 ms time intervals after induction of a single DSB. (**E**) Time and ensemble MSD of the *tet*O locus measured with a 500 ms exposure time at 1000 ms time intervals after induction of a single DSB. The dotted line displays the fit of the MSD curve at 1000 ms time intervals using the same *A* and $\alpha$ found at 10 and 100 ms time intervals (A = 0.006 and a = 0.5). Again, only a different anomalous regime could fit the MSD (shown in plain lines). (**F**) Merge of the 3 time scales (Fig.3C, 3D and 3E) plotted in log-log scale

showing three different regimes (red: presence of a single DSB). The log-log MSD curves from Fig. 2F are also shown (black: absence of a DSB).

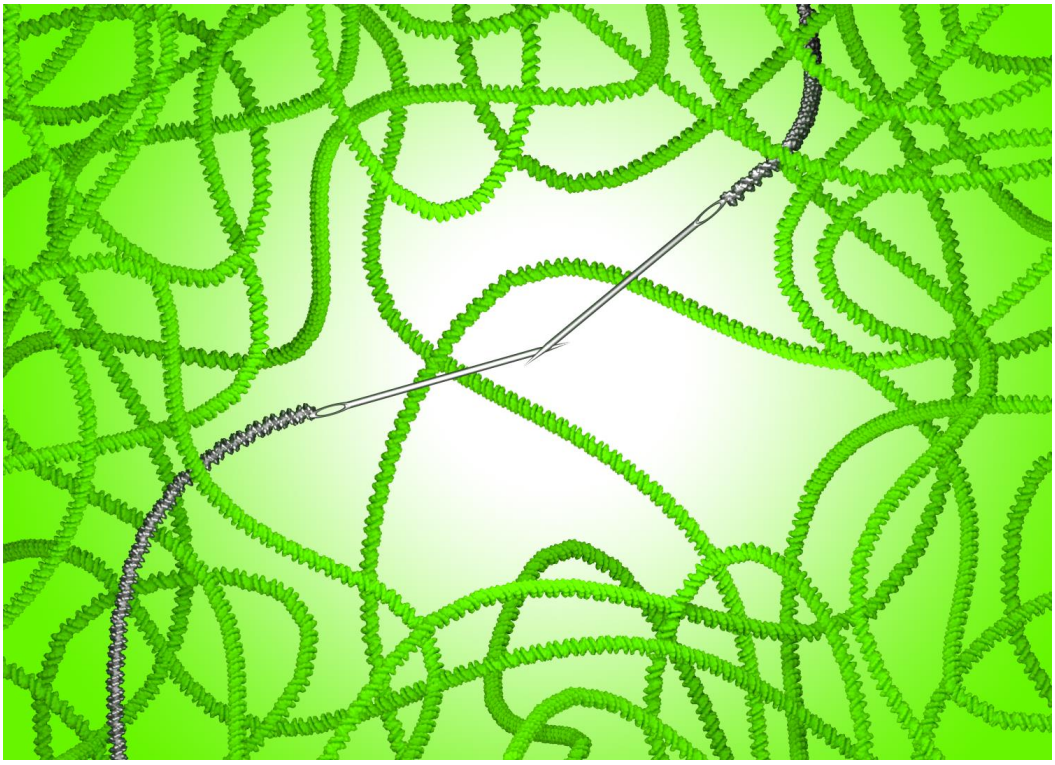

**Figure 4. "Needle in a ball of yarn" model**

To explain how damaged DNA ends exhibit decreased mobility at short time scales and simultaneously increased mobility at longer time scales, we propose the following model that we name "needle in a ball of yarn." In response to DNA damage, the repair complex forms a nucleo-filament on the single strand DNA tail, which stiffens the damaged end, thus decreasing its mobility locally. However, the same stiffened DNA end acts like a needle in a ball of yarn, enabling it to bypass the DNA meshwork and escape adjacent obstacles more efficiently, thus increasing mobility at longer time scales. The two ends are represented as searching together consistent with (Lisby et al., 2003, Lobachev et al., 2004, Kaye et al., 2004).

**TABLE 1: Summary of anomalous motions measured in this study**

The anomalous diffusion coefficients $A$ and the anomalous exponents α were obtained by fitting the MSD curves with $At^{\alpha} + b$ (see equation 1 from Supplementary Text 1). The parameter $b$ is an experimental offset allowing the correction of artifacts during the acquisition (i.e., localization accuracy and motion blur, see Supplementary Text 1). The fitting method is described in details in Supplementary Text 2. For clarity, we present the errors on parameters $A$ and $\alpha$ in Supplementary Table 1.

| | **Haploid, no DSB** | | | **Diploid, no DSB** | | | **Diploid, damaged locus** | | |
|---|---|---|---|---|---|---|---|---|---|
| **Time intervals** | 10 ms | 100 ms | 1000 ms | 10 ms | 100 ms | 1000 ms | 10 ms | 100 ms | 1000 ms |
| ***A*** | 0.011 | 0.012 | 0.012 | 0.0075 | 0.0075 | 0.0064 | 0.0065 | 0.006 | 0.0087 |
| ***α*** | 0.38 | 0.50 | 0.50 | 0.50 | 0.50 | 0.49 | 0.50 | 0.50 | 0.58 |

**Supplementary Movie S1:**

Haploid S-phase cells with *tetO*/TetR-RFP locus at the *URA3* locus and a Spc110-YFP focus in the same focal plane. The movie is recorded in 2 dimensions with 50 ms exposure time in the RFP channel followed by 50 ms exposure time in YFP. The lines indicate the trajectories obtained after image analysis of each spot.

# SUPPLEMENTARY

**Supplementary Figure S1**

**The MSD is anomalous at the time scales examined**

Anomalous movement has sometimes been wrongly referred to as confined. Here, we perform three methods of analysis to support the anomalous nature of the motion.

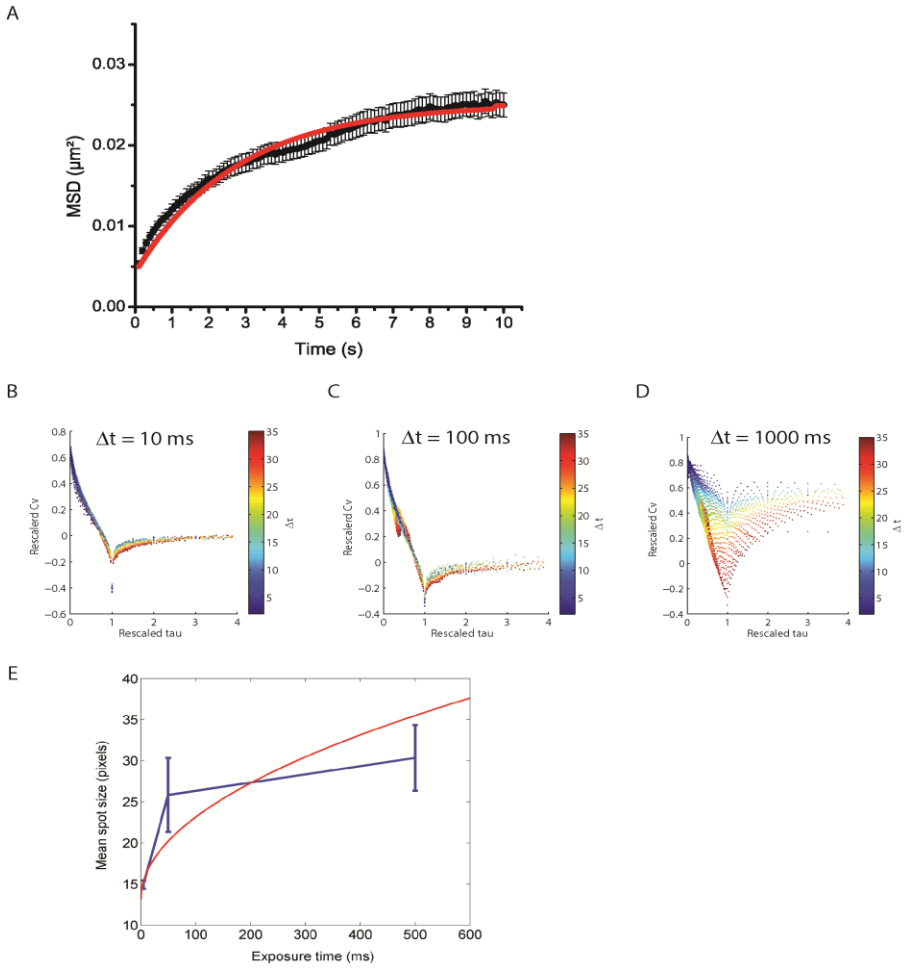

(**A**) **Method 1**: we fitted the experimental MSD with an exponential decay function ($MSD = cst\ (1 - e^{(x-x_0)/\tau}$). This function exhibits a clear plateau that characterizes confined motion inside a sub-nuclear volume. Here, we test the plateau hypothesis for the experimental condition with the larger dataset: 100 ms time intervals for diploid cells (11 cells analyzed, more than 5000 time points). We fitted the time-ensemble MSD curve with the following exponential decay function ($MSD = cst\ (1 - e^{(x-x_0)/\tau}$) and we obtain a typical R2 = 0.975. The fit of the same experimental MSD curve with a power law is clearly better (R2 = 0.996, Fig.2D) supporting the anomalous sub-diffusion nature of DNA motion for this condition. The same test was performed for each condition and we always obtained a less accurate fit with an exponential decay function than with a power law (data not shown).

(**B**) (**C**) and (**D**) **Method 2**: for haploid cells, we calculated the velocity auto-correlation (VAC), a function that is shown to be scale-less only in the case of anomalous diffusion (Weber et al., 2012b). The VAC, $Cv(\Delta t)$, is the correlation between two velocities $\vec{v}$ separated by a time interval Δt: $Cv(\Delta t) = \langle v(t+\Delta t) \cdot v(t) \rangle$. The velocity $(t)$ is the displacement of the locus calculated during time δ. As proposed by Weber *et al.* (2012b), to represent the VAC, we plot the VAC as a function of a non-dimensional quantity, rescaled tau, defined as $\frac{\Delta t}{\delta}$. Rescaled tau is a fraction of time that separates two correlated velocities. When rescaled tau = 1, the estimated correlation is done between consecutive velocities; when rescaled tau = 2, the time interval between 2 velocities to correlate (Δt) is twice as large as the time (δ) over which the velocity is measured; in other words, the correlation is calculated every $2v$. A positive auto-correlation $Cv$ indicates that, on average, the compared velocities share the same direction; a null auto-correlation indicates that their directions are independent; finally, a negative auto-correlation indicates that the 2 velocities have opposite directions. For free Brownian diffusion without any experimental artifacts, the motion has no memory and we expect a VAC equal to zero if the velocities do not have an overlap in time (rescaled tau ≥ 1). Figures S1B, S1C and S1D display the VAC of the *URA3* locus in diploid cells observed at 10, 100 and 1000 ms time intervals, respectively, as a function of the rescaled tau. Weber *et al.* showed that for anomalous sub-diffusion, the auto-correlation of the velocities is scale-less regardless of pointing accuracy (Weber et al., 2012b). The VAC functions are calculated for time intervals Δt varying from 0 to 35 time-points, the colors of the curves representing Δt. In figures S1B and S1C, the VAC curves overlay very well as

shown by the overlapping curves in different colors. For 1000 ms time intervals however, the 3D movement makes the 2D modeling of the localization accuracy inaccurate and the scale less nature of the recorded displacement is less good (Fig. S1D).

(**E**) **Method 3**: we calculated the mean size of the detected spot of the tagged locus as a function of the exposure time. If the locus stays in focus, this area is proportional to the space explored convoluted with the point spread function of an immobile locus. In the case of normal diffusion, since the space explored is proportional to time, the mean size of the *URA3* spots is supposed to scale linearly. Here, the concave curve indicates that the locus motion is not a normal diffusion.

**Supplementary Text 1: Fit of a power law on a MSD curve taking into account exposure time**

The MSD is a standard statistical tool that describes a set of trajectories of similar objects. However, numerous artifacts perturb this statistic. The localization accuracy can have a strong impact on the MSD curve, even computed on simple Brownian motion (Saxton and Jacobson, 1997). Considering the movement of a single photon emitter, the localization accuracy can be divided into:

i) The error in the determination of the accurate particle position due to convolution with the point spread function (PSF) and the finite number of photons. This error is more important for short acquisition times since the number of photons collected is small.

ii) The error due to the movement of the particle during the camera acquisition. This error is more important with higher exposure times and is sometimes referred to as "motion blur".

For 2D Brownian motion with a diffusion coefficient D, Michalet computed the formula of the converged MSD including the corrections for localization accuracy (Michalet, 2010):

$$MSD(t) = 4Dt + \sigma_0^2\left(1 + \frac{Dt_E}{s_0^2}\right) - \frac{4}{3}Dt_E$$

where $\sigma_0^2$ : localization accuracy of an immobile particle,

$s_0^2$ is the variance of the PSF,

$t_E$ is the exposure time of the camera.

The term 4D*t* is the theoretical MSD for simple Brownian motion. The term $\sigma_0^2\left(1 + \frac{Dt_E}{s_0^2}\right)$ accounts for the *motion blur* of the particle along its path during acquisition. Since the localization accuracy $\sigma_0^2$

is inversely proportional to the number of collected photons, we have $\sigma_0^2 \propto \frac{1}{t_E}$. The motion blur term therefore converges to a fixed value as the exposure time increases. The term $\frac{4}{3}Dt_E$ accounts for the correlation between successive displacements due to the exposure overlap.

Since here we show that DNA motion is well described by anomalous diffusion, we compute the MSD of an anomalously moving molecule by including the corrections for the localization accuracy and the exposure time. Anomalous diffusion is defined by a theoretical MSD proportional to a power of the time: $MSD = A\,t^{\alpha}$. The value of the anomalous exponent is usually found by a mean square linear regression of the experimental MSD curve in log-log scale. Using the approach proposed by Michalet (Michalet, 2010), we find at the second order approximation:

$$MSD(t) = At^{\alpha} + \sigma_0^2\left(1+\frac{At_E^{\alpha}}{4s_0^2}\right) - \frac{A\alpha(1-\alpha)t_E^2}{12t^2}t^{\alpha} - \frac{2A}{(\alpha+1)(\alpha+2)}, \text{ equation 1}$$

The term $\sigma_0^2\left(1+\frac{At_E^{\alpha}}{4s_0^2}\right)$ still accounts for the motion blur, but has a fundamental difference compared to its normal diffusion equivalent: as $t_E$ increases, it is equivalent to $t_E^{\alpha-1}$ and therefore, in the case of sub-diffusion, the blur influence is decreased for high exposure time. Because of constant resampling of its environment, the average position of the anomalously moving particle is known more accurately for longer exposure times. Similarly, the term $\frac{A\alpha(1-\alpha)t_E^2}{12t^2}t^{\alpha}$ quickly disappears with speed $t^{\alpha-2}$ leaving only the term $\frac{2A}{(\alpha+1)(\alpha+2)}$. We tested our formula on two theoretical anomalous diffusion models: Fractional Brownian Motion (FBM) (Ben-Avraham, 2000) and a random walk in a maximum 2D site percolation cluster (Ben-Avraham, 2000) and find that the formula is in very good agreement with our simulations (see Fig. S2).

When fitting an MSD curve to a power law $MSD = At^{\alpha} + b$, the offset term $b$ can be significantly

negative and its value can have a strong impact on the estimated α. The protocol that gives the best results on simulation is the following: we estimated an approximate value of the anomalous coefficient α using a least square linear regression of the experimental for the simple $MSD(t) = At^{\alpha`}$ . We then estimated the motion blur effect, $MB = \frac{2A}{(\alpha+1)(\alpha+2)}$, and found $\alpha$ and $A$ fitting the MSD curves to the formula $MSD(t) = b' + At^{\alpha}$ with $b'$ taking discrete values in the interval: $[-MB;+MB]$. We then found the estimates that displayed the best $R^2$ value.

Finally, we estimated the motion blur and localization error defined by $\sigma_{err} = \sigma\sqrt{1+\frac{At_E^{\alpha}}{4s_0^2}}$ for all the different studied condition:

| | $t_E$ | $\sigma_{err}$ |
|---|---|---|
| Haploid | $t_E$ = 5 ms | 100 nm |
| | $t_E$ = 50 ms | 90 nm |
| | $t_E$ = 500 ms | 120 nm |
| Diploid | $t_E$ = 5 ms | 80 nm |
| | $t_E$ = 50 ms | 90 nm |
| | $t_E$ = 500 ms | 80 nm |
| DSB induced | $t_E$ = 5 ms | 70 nm |
| | $t_E$ = 50 ms | 90 nm |
| | $t_E$ = 500 ms | 120 nm |

This method gives an average localization accuracy of 90 nm.

**Supplementary Figure S2: Effect of exposure time on the MSD of an anomalously moving molecule.**

As described in Supplementary Text 1, the theoretical MSD of anomalous motion follows a power law, $MSD(t) = At^{\alpha}$; however, due to acquisition artifacts, an experimental MSD follows $MSD(t) = At^{\alpha} + b$, where b is an offset term (see equation 1). Here, we tested the term accounting for motion blur $MB = \frac{2A}{(\alpha+1)(\alpha+2)}$ calculated in equation 1 using simulations. To do that, we first simulated the motion of an anomalous particle using two physical models leading to anomalous diffusion: the Fractional Brownian Model (FBM) and a random walk in a maximum 2D site percolation cluster (Fig. S2A and S2B, respectively). From these simulated trajectories, we calculated their corresponding MSD in 2 different ways: i) the MSD is calculated using all the simulated positions of the particle (Fig. S2C and S2D, black curves), ii) the MSD is calculated after averaging the positions of the particle over 10 time-points to mimic a 10 times longer exposure time of a camera (Fig. S2C and S2D, red curve referred as "MSD averaged" in the figures). The difference between the MSD and the "MSD averaged" is the offset term due to motion blur. We then compared the offset obtained from these simulated trajectories with the offset predicted by equation 1 (bottom of Fig. S2C and S2D).

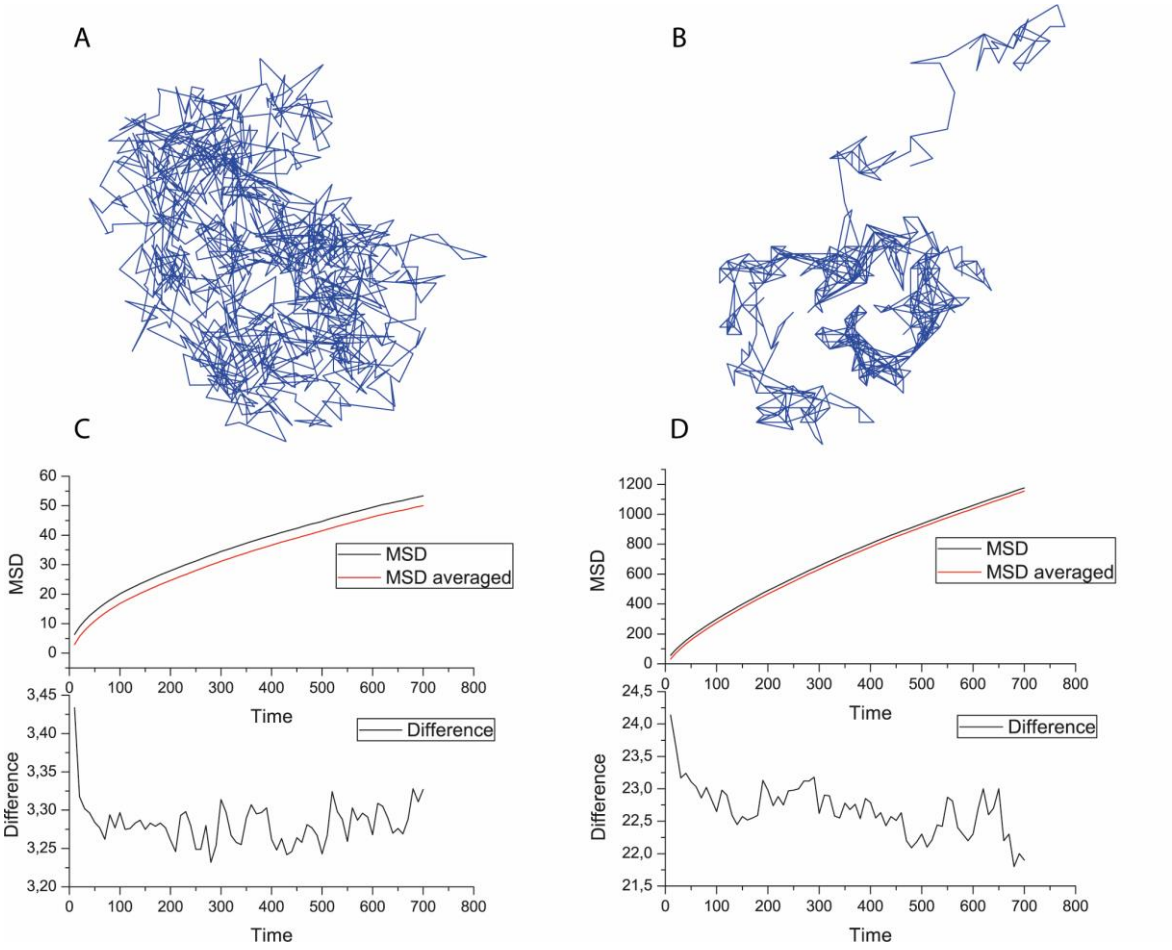


(**A**) Example of a trajectory obtained by simulating FBM in 2D.

(**B**) Example of a trajectory obtained by simulating a random walk in a maximum 2D site percolation cluster.

(**C**) Time and ensemble MSD of FBM trajectories. MSD of FBM is characterized by the anomalous expression: $MSD = 2\,t^{0.5}$ (Hughes, 1995). We used our simulations of FBM to validate the offset terms due to motion blur during the acquisition in equation 1. Black curve: the MDS is computed

directly on the FMB simulated trajectories. Red curve: the MSD is computed on trajectories with positions averaged over 10 points to simulate a 10 times longer exposure time of the camera. The difference between the MSD and the averaged MSD represents the effects of motion blur on the MSD and is $2.34 \pm 0.2$ (bottom of Fig. S2C). Importantly, the predicted offset calculated from equation 1 is $\frac{2A}{(\alpha+1)(\alpha+2)} \approx 3.37$, a value extremely close to the value obtained by simulation.

(D) To strengthen our method, we performed the same study using a different type of model that also leads to anomalous motion: a random walk in a maximum 2D site percolation cluster with $MSD(t) = At^{\alpha} \approx 10.8t^{0.71}$. Equation 1 predicts that the difference due to the motion blur between the theoretical and the experimental MSD is $\frac{2A}{(\alpha+1)(\alpha+2)} \approx 23.9$. Again, these simulations predict the same difference between the theoretical and the experimental MSD (bottom of Fig. S2D).

Overall, we simulated the motion of a particle using two different models of anomalous diffusion; we then computed their MSDs using either all the obtained particle positions (MSD, black curves) or the averaged positions over 10 time-points to simulate a 10 times longer exposure time (MSD averaged, red curves). Comparing the MSDs and the MSDs averaged, we estimate the offset term due to the motion blur and find a value extremely close to the one obtained from equation 1, which validates our analytical approach.

**Supplementary Text 2: Finding the anomalous exponent**

We tested 2 methods to fit the experimental MSD curves.

First fitting method: α not constrained

We first fitted the ensemble MSD with free *A* and $\alpha$ parameters in $MSD(t) = At^{\alpha} + b$ using equation 1 described in Supplementary Text 1. For example, we find the following anomalous exponents: 0.38, 0.44 and 0.39 for haploid cells (R2= 0.998, 0.996 and 0.994 respectively), very close to the 0.42 exponent found by Weber *et al*. (Weber et al., 2012a). However, we observe an important cell-to-cell variability (Fig. S3A, B and C). The 95% confidence interval of the anomalous exponents of individual cells is about +/-0.15. To investigate whether this large confidence interval is due to a too low number of cells analyzed or to cell-to-cell variability, we evaluated how the anomalous exponent converges as a function of the number of cells analyzed using a bootstrap method (Fig. S3D, E and F). For each condition, we randomly picked several cells 100 times and evaluated the averaged corresponding anomalous exponent. We found that the number of cells analyzed is not responsible for the large confidence interval since the anomalous exponent rapidly converges. For that reason, we propose that the large confidence interval is due to an important cell-to-cell variability.

Second fitting method: α constrained

We next fitted the same ensemble MSD with a free *A* parameter, but fixed the anomalous exponent $\alpha$ to 0.5 as proposed by Hajjoul *et al (Hajjoul et al., 2013)*. Using equation 1 from Supplementary Text 1, we found a satisfactory fit for 100 and 1000 ms time intervals with MSD(t) = 0.012 $t^{0.5}$ (R2=0.995 and 0.996, Fig. 1D and 1E). This value is very similar to MSD(t) = 0.011 $t^{0.5}$ obtained in (Hajjoul et al., 2013). Importantly, fixing the anomalous exponent to 0.5 did not affect the quality of the fit, as shown by the very small R2 decrease between the 2 fitting methods (e.g., at 100 ms time intervals: R2 = 0.996 with the unconstrained fit and R2 = 0.995 with the constrained fit; at 1000 ms time intervals, R2 = 0.994 and R2 = 0.996, with the unconstrained and constrained fit respectively). Surprisingly however, in some cases, DNA mobility failed to follow that regime (haploids imaged a 10 ms time intervals, Fig. 1C and damaged diploids imaged at 1000 ms time intervals, Fig. 3E). In these cases, fixing the anomalous exponent to 0.5 does not give an acceptable fit (R2 = 0.974 constrained): we thus used the unconstrained fitting method described above and found MSD = 0.011 $t^{0.38}$, R2 = 0.999 for haploids at 10 ms time intervals, and MSD = 0.0087 $t^{0.58}$ for damaged diploids at 1000 ms time intervals.

**Supplementary Table 1**: Anomalous exponents and anomalous diffusion coefficients found in this study, with standard deviations. The error on parameters $A$ and $\alpha$ is the standard deviation of the fit.

| | **Haploid, no DSB** | | | **Diploid, no DSB** | | | **Diploid, damaged locus** | | |
|---|---|---|---|---|---|---|---|---|---|
| **Time intervals** | 10 ms | 100 ms | 1000 ms | 10 ms | 100 ms | 1000 ms | 10 ms | 100 ms | 1000 ms |
| ***A*** | 0.011 $\pm$ 0.001 | 0.012 $\pm$ 0.001 | 0.012 $\pm$ 0.001 | 0.0075 $\pm 5.10^{-4}$ | 0.0075 $\pm 5.10^{-4}$ | 0.0064 $\pm 5.10^{-4}$ | 0.0065 $\pm 5.10^{-4}$ | 0.006 $\pm$ 0.001 | 0.0087 $\pm 5.10^{-4}$ |
| ***α*** | 0.38 $\pm$ 0.02 | 0.50* | 0.50* | 0.50* | 0.50* | 0.49 $\pm$ 0.01 | 0.50* | 0.50* | 0.58 $\pm$ 0.01 |

*this anomalous exponent was determined with a constrained fit on $\alpha$ (with similar R2 than unconstrained fit, see Supplementary Text 2).

**Supplementary Figure S3: Cell variability**

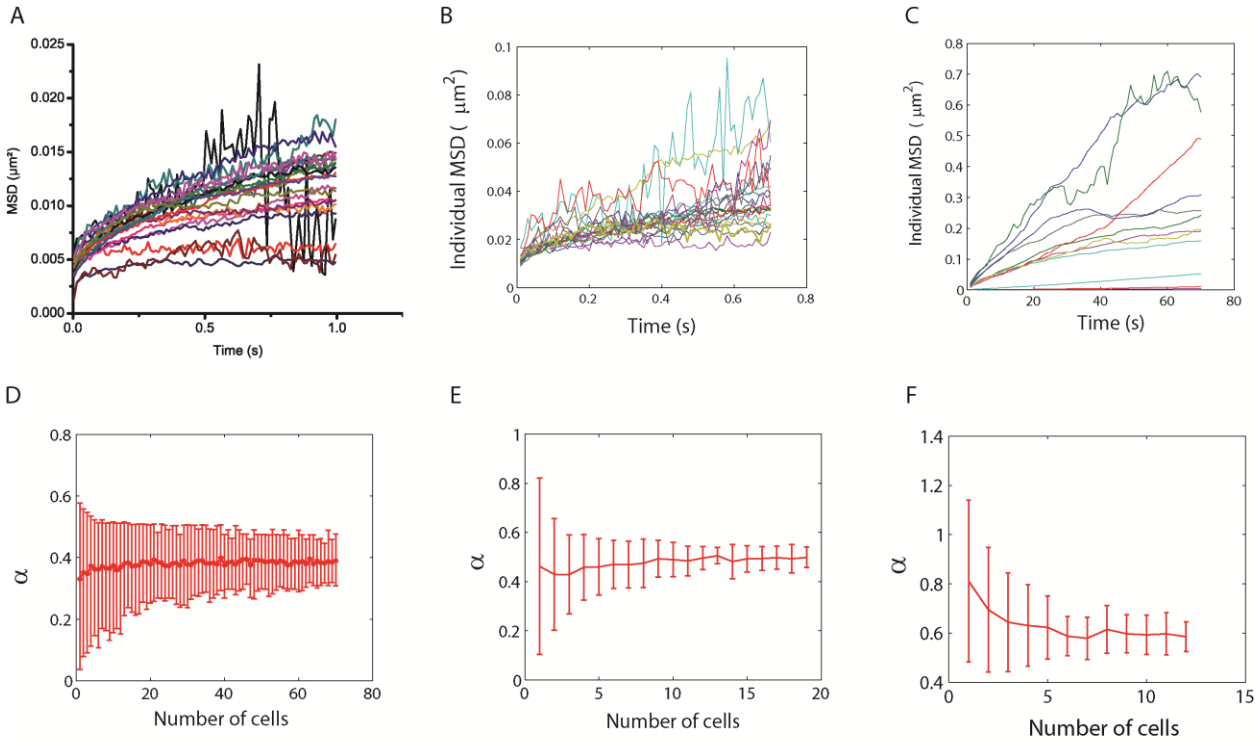


(**A**) MSDs of individual haploid cells observed at 10ms time intervals. (**B**) and (**C**): MSDs of individual diploids observed at 100 and 1000ms time intervals, respectively. The cell heterogeneity possibly reflects different chromatin organization inside the nucleus.

(**D**), (**E**), (**F**) Anomalous exponents α extracted from individual MSD curves as a function of the number of cells analyzed. Trajectories are composed of approximately 400 successive time points during cell imaging. We use a "bootstrap approach" to estimate the proper number of trajectories that should be analyzed to obtain a robust anomalous exponent. To do that, a certain number of trajectories is randomly drawn (*x* axis) and their corresponding ensemble-averaged MSD and anomalous exponent is calculated. The draw is performed 100 times over our set of acquired trajectories and we show the mean anomalous exponent obtained as function of the number of trajectories drawn (*y* axis). The error bars are the 5% and 95% bootstrap interval of the anomalous exponent α. We found that the anomalous exponent α converges rapidly while the error bars stay large. This result indicates that our dataset is large enough to provide a robust anomalous exponent and the large error bar is due to cell heterogeneity.

**Supplementary Table S2**: yeast strains used in this study (Mine-Hattab & Rothstein, 2012).

| | |
|---|---|
| U3145 | *MATα ade2-1 leu2-3,112 ura3-1::URA3-LacOx256 lys2Δ RAD52-CFP his3-11,15::YFP-LacI-197K-HIS3* |
| W8836-5D | *MAT***a** *ade2-1 his3-11,15 leu2-3,112 trp1-1 ura3-1::3xURA3-TetOx112 I-SceIcs(ura3-1) TetR-mRFP1(iYGL119W)* |
| W9410 | U3145 x W8836-5D |
| W9561-17A | *MAT***a** *ADE2 lys2::GAL-I-SceI ura3-1::3xURA3-TetOx112 I-SceIcs(ura3-1) TetR-mRFP1(iYGL119W) trp1-1 leu2-3,112 his3-11,15* |
| W9593 | U3145 x W9561-17A |
| W9562-1A | *MAT***a** *ADE2 his3-11,15::SPC110-YFP-HIS3 ura3-1::3xURA3-TetOx112 I-SceIcs(ura3-1) TetR-mRFP1(iYGL119W) bar1::LEU2 lys2::GAL-I-SceI trp1-1* |
| W9641 | U3145 x W9562-1A |
| U3199 | *MAT***a** *ADE2 lys2::GAL-I-SceI ura3-1::3xURA3-tetOx112 I-SceI(ura3-1) TetR-mRFP1(iYGL119W) trp1-1 leu2-3,112 his3-11,15 rad51Δ::KAN* |
| U3174 | *MAT***a** *ADE2 his3-11,15::SPC110-YFP-HIS3 ura3-1::3xURA3-tetOx112 I-SceI(ura3-1) TetR-mRFP1(iYGL119W) bar1::LEU2 lys2::GAL-I-SceI trp1-1 rad51Δ::KAN* |
| U3198 | *MATα ade2-1 leu2-3,112 ura3-1::URA3-LacOx256 lys2Δ Rad52-CFP his3-11,15::YFP-LacI-197K-HIS3 rad51Δ::KAN* |
| W9897 | U3199 x U3198 |
| W9898 | U3174 x U3198 |
| W9530-21C | *MATα ade2-1 ura3-1::3xURA3-tetOx112 I-SceI(ura3-1) TetR-mRFP1(iYGL119W) lys2::GAL-I-SceI Rad52-CFP bar1::LEU2 trp1-1 his3-11,15* |
| W9387-20A | *MAT***a** *ADE2 his3-11,15::SPC110-YFP-HIS3 leu2-3,112 ura3-1 trp1-1* |
| W9562 | W9530-21C x W9387-20A |

**REFERENCES:**

Ben-Avraham, D.H., S. (2000). Diffusion and reactions in fractals and disordered systems Cambridge University Press.

Hajjoul, H., Mathon, J., Ranchon, H., Goiffon, I., Mozziconacci, J., Albert, B., Carrivain, P., Victor, J.M., Gadal, O., Bystricky, K., *et al.* (2013). High-throughput chromatin motion tracking in living yeast reveals the flexibility of the fiber throughout the genome. Genome research *23*, 1829-1838.

Hughes, B.D. (1995). Random Walks and Random Environments: Volume 1: Random Walks. Oxford science publications.

Michalet, X. (2010). Mean square displacement analysis of single-particle trajectories with localization error: Brownian motion in an isotropic medium. Physical review. E, Statistical, nonlinear, and soft matter physics *82*, 041914.

Saxton, M.J., and Jacobson, K. (1997). Single-particle tracking: applications to membrane dynamics. Annual review of biophysics and biomolecular structure *26*, 373-399.

Weber, S.C., Spakowitz, A.J., and Theriot, J.A. (2012a). Nonthermal ATP-dependent fluctuations contribute to the in vivo motion of chromosomal loci. Proc Natl Acad Sci U S A *109*, 7338-7343.

Weber, S.C., Thompson, M.A., Moerner, W.E., Spakowitz, A.J., and Theriot, J.A. (2012b). Analytical tools to distinguish the effects of localization error, confinement, and medium elasticity on the velocity autocorrelation function. Biophys J *102*, 2443-2450.